

This is a repository copy of *Geometric morphometrics and finite elements analysis: Assessing the functional implications of differences in craniofacial form in the hominin fossil record*.

White Rose Research Online URL for this paper:

<https://eprints.whiterose.ac.uk/127295/>

Version: Accepted Version

Article:

O'Higgins, Paul orcid.org/0000-0002-9797-0809, Fitton, Laura C. orcid.org/0000-0003-4641-931X and Godinho, Ricardo Miguel (2017) Geometric morphometrics and finite elements analysis: Assessing the functional implications of differences in craniofacial form in the hominin fossil record. *Journal of archaeological science*. ISSN 0305-4403

<https://doi.org/10.1016/j.jas.2017.09.011>

Reuse

Items deposited in White Rose Research Online are protected by copyright, with all rights reserved unless indicated otherwise. They may be downloaded and/or printed for private study, or other acts as permitted by national copyright laws. The publisher or other rights holders may allow further reproduction and re-use of the full text version. This is indicated by the licence information on the White Rose Research Online record for the item.

Takedown

If you consider content in White Rose Research Online to be in breach of UK law, please notify us by emailing eprints@whiterose.ac.uk including the URL of the record and the reason for the withdrawal request.

1
2
3
4
5
6
7
8
9
10
11
12
13
14
15
16
17
18
19
20
21
22

Geometric morphometrics and Finite elements analysis: Assessing the functional implications of differences in craniofacial form in the hominin fossil record

Paul O'Higgins^a, Laura C Fitton^a and Ricardo Miguel Godinho^a

Paul O'Higgins (corresponding author)

a) Hull York Medical School and Department of Archaeology of the University of York
John Hughlings Jackson Building, University of York, Heslington, York YO10 5DD, UK
paul.ohiggins@hyms.ac.uk

Laura C. Fitton

Hull York Medical School and Department of Archaeology of the University of York
John Hughlings Jackson Building, University of York, Heslington, York YO10 5DD, UK
laura.fitton@hyms.ac.uk

Ricardo Miguel Godinho¹

a) Hull York Medical School and Department of Archaeology of the University of York
Academic address: John Hughlings Jackson Building, University of York, Heslington, York
YO10 5DD, UK

b) Interdisciplinary Center for Archaeology and Evolution of Human Behaviour (ICArHEB)
Faculdade das Ciências Humanas e Sociais, Universidade do Algarve, Campus Gambelas,
8005-139, Faro, Portugal

¹ Permanent address: R. Dr. Joaquim Fiadeiro, nº86, Urbanização Tapada do Carapetal, 7200-480 Reguengos de Monsaraz, Portugal

23 ricardomiguelgodinho@gmail.com

24

25

26 **Abstract:**

27 The study of morphological variation in the hominin fossil record has been transformed in
28 recent years by the advent of high resolution 3D imaging combined with improved geometric
29 morphometric (GM) toolkits. In parallel, increasing numbers of studies have applied finite
30 elements analysis (FEA) to the study of skeletal mechanics in fossil and extant hominoid
31 material. While FEA studies of fossils are becoming ever more popular they are constrained
32 by the difficulties of reconstruction and by the uncertainty that inevitably attaches to the
33 estimation of forces and material properties. Adding to these modelling difficulties it is still
34 unclear how FEA analyses should best deal with species variation.

35 Comparative studies of skeletal form and function can be further advanced by applying tools
36 from the GM toolkit to the inputs and outputs of FEA studies. First they facilitate virtual
37 reconstruction of damaged material and can be used to rapidly create 3D models of skeletal
38 structures. Second, GM methods allow variation to be accounted for in FEA by warping
39 models to represent mean and extreme forms of interest. Third, GM methods can be applied
40 to compare FEA outputs – the ways in which skeletal elements deform when loaded. Model
41 comparisons are hampered by differences in material properties, forces and size among
42 models but how deformations from FEA are impacted by these parameters is increasingly
43 well understood, allowing them to be taken into account in comparing FEA outputs.

44 In this paper we review recent advances in the application of GM in relation to FEA studies
45 of craniofacial form in hominins, providing examples from our recent work and a critical
46 appraisal of the state of the art.

47

48 **Keywords:** Form-function; Geometric Morphometrics; Finite Element Analysis; Craniofacial
49 form; Functional performance.

50

51

52 **1. Introduction**

53 In this paper we consider how the mechanical performance of crania in biting can be
54 estimated and compared among fossils, paying particular attention to how the methods of
55 geometric morphometrics (GM) can facilitate such analyses in combination with
56 biomechanical modelling using finite elements analysis (FEA).

57

58 As with other skeletal elements, crania fulfil mechanical functions, such as housing and
59 protection of organs and provision of a rigid framework for food acquisition and intra-oral
60 processing by the masticatory apparatus (Lieberman, 2011), which comprises jaws, teeth and
61 soft tissues. Thus, much research has focused on the association between cranial form and
62 masticatory function, with the aims of understanding how crania function and how their
63 functional abilities (performances) differ among related species. These differences have
64 underpinned investigations of how skeletal form, function, ecology and behaviour interrelate
65 (Groning, et al., 2011b, Rayfield, 2005, Rayfield, 2007, Rayfield, et al., 2001, Strait, et al.,
66 2010, Strait, et al., 2007, Strait, et al., 2009, Wroe, et al., 2010, Wroe, et al., 2007). In turn,
67 knowledge of these interrelationships has been used to infer ecology and behaviour from
68 skeletal remains of extinct taxa (Attard, et al., 2014, Cox, et al., 2015, Degrange, et al., 2010,
69 Ledogar, et al., 2016, Oldfield, et al., 2012, Rayfield, 2005, Rayfield, et al., 2001, Smith, et
70 al., 2015b, Strait, et al., 2010, Strait, et al., 2009, Wroe, 2008).

71

72 One aspect of performance, bite force, can be directly measured in extant species using force
73 transducers. These have been widely used to measure bite forces in living humans (Braun, et
74 al., 1995, Kikuchi, et al., 1997, Paphangkorakit and Osborn, 1997, Sinn, et al., 1996). In
75 extinct material alternative approaches are required to estimate forces from skeletal evidence,
76 using bony proxies to approximate lever arm lengths and maximum muscle forces based on
77 the relationships between muscle area, intrinsic muscle fibre strength and force production
78 (Gans and de Vree, 1987, Josephson, 1975, Weijjs, 1980). Although this provides an estimate
79 of the force produced by muscles it ignores pennation and depends on the validity of the
80 estimates of muscle areas from bony proxies. Muscle force is converted into bite force
81 through the masticatory lever arm system. By measuring in and out-levers of the masticatory
82 system and computing their ratios, it is possible to estimate the mechanical efficiencies of
83 each muscle and to estimate maximal bite forces (Antón, 1990, Demes and Creel, 1988, Eng,

84 et al., 2013, O'Connor, et al., 2005). However, this approach has limitations due to
85 differences between the cross sectional areas estimated via bony proxies and actual
86 physiological muscle cross sectional areas (Eng, et al., 2013, Toro-Ibacache, et al., 2015), and
87 because the lever system of the jaws is often simplified to two dimensions to ease
88 calculations. Bite force can also be predicted using FEA (Wroe, et al., 2010) and by
89 multibody dynamic analysis (MDA) (Bates and Falkingham, 2012, Curtis, et al., 2008, Shi, et
90 al., 2012). MDA can also be used to infer muscle activation patterns given a particular load.
91 These approaches take full account of the three dimensional geometry of the masticatory
92 lever system but retain dependence on the accuracy of input of variables, such as muscle
93 forces, force vector directions and cranial geometry.

94 Bite forces are transmitted to items held between the teeth, and the teeth and cranium
95 experience the bite reaction force. Thus, crania have to be adapted to withstand masticatory
96 forces. In order to assess, explain and compare how the cranium resists occlusal forces,
97 researchers have used several approaches. These include the analysis of simplified
98 biomechanical models of craniofacial anatomy considered in terms of vertical and horizontal
99 column-like structures that buttress the face and channel bite reaction forces (Görke, 1904;
100 Richter, 1920; Endo, 1965; Endo, 1966) and models that consider crania as a cylinder that is
101 twisted during biting (Greaves, 1985; Greaves and Mucci, 1997; Demes, 1987). These
102 models and their underlying assumptions have been tested through the application of strain
103 gauges to directly measure the surface strains experienced during biting (Hylander et al.,
104 1991; Hylander et al., 1992; Ross and Hylander, 1996; Ravosa et al., 2000a; Ravosa et al.,
105 2000b; Ross, 2001; Ross et al., 2011). FEA has also been applied to this task (Ledogar, et al.,
106 2016, Smith, et al., 2015b, Strait, et al., 2010, Strait, et al., 2007, Strait, et al., 2009, Wroe, et
107 al., 2010) but an important issue in such studies is validity of FEA results, do they match
108 reality?

109

110 For this reason validation studies have been carried out to assess the accuracy of prediction of
111 cranial and mandibular deformations, comparing measured with predicted strains (Bright and
112 Groning, 2011, Groning, et al., 2009, Kupczik, et al., 2007, Ross, 2005, Toro-Ibacache, et al.,
113 2016). In so doing, researchers can assess how various input parameters including skeletal
114 geometry, material properties, constraints, applied forces etc. impact FE model results in
115 order to create more realistic models (Ross, 2005, Strait, et al., 2005, Toro-Ibacache, et al.,
116 2016). In general validation studies tell us that accurate strain prediction in any one specimen
117 is difficult and requires careful adjustment of model parameters to achieve valid results.

118

119 The accuracy of predictions achieved by FEA is, however, entirely dependent on these input
120 parameters, so, acknowledging modelling limitations, researchers have sought to understand
121 the impact of variations and simplifications in FE modelling. This has led to sensitivity
122 studies in which the impact on predicted deformations of varying specific parameters is
123 assessed. Such parameters include the muscle force magnitudes, directions and activation
124 patterns (Cox, et al., 2011, Fitton, et al., 2012, Groning, et al., 2012, Ross, 2005, Sellers and
125 Crompton, 2004), variations in material properties (Cox, et al., 2011, Groning, et al., 2012,
126 Kupczik, et al., 2007, Reed, et al., 2011, Strait, et al., 2005, Toro-Ibacache, et al., 2016),
127 modelling cranial sutures (Kupczik, et al., 2007, Reed, et al., 2011, Wang, et al., 2010),
128 simplifications in model geometry (Fitton, et al., 2015, Toro-Ibacache, et al., 2016),
129 modelling the periodontal ligament (Groning, et al., 2012, Holland, 2013, McCormack, et al.,
130 2014, Wood, et al., 2011), impact of variations in modelling of trabecular bone (Parr, et al.,
131 2013) and model constraints (Cox, et al., 2011). Validation and sensitivity studies have
132 shown that modelling variations that affect model stiffness (e.g. bone thicknesses, how
133 cancellous bone is represented, material properties, etc.) or total applied force tend to lead to
134 differences in magnitude rather than mode of deformation, while variations in relative muscle
135 activations, muscle vectors and constraints tend to impact mode of deformation, how the
136 cranium deforms (Fitton, et al., 2015, Godinho, et al., 2017, Parr, et al., 2012, Toro-Ibacache,
137 et al., 2016).

138

139 Researchers have tried to predict how fossil hominin crania resist biting. Such analyses have
140 until recently relied on geometrical simplifications of crania (Demes, 1987, Rak, 1983, Rak,
141 1986, Trinkaus, 1987). More recently, FEA has been used to more fully model fossil hominin
142 masticatory biomechanics with the aim of improving prediction of the stresses and strains
143 experienced by fossil crania as they deform during biting (Ledogar, et al., 2016, Smith, et al.,
144 2015b, Strait, et al., 2010, Strait, et al., 2009, Wroe, et al., 2010). Sensitivity studies are of
145 particular relevance here as validation is not possible for fossils. FEA applied to fossils has
146 become popular (Cox, et al., 2011, Cox, et al., 2012, Rayfield, 2007, Strait, et al., 2013,
147 Strait, et al., 2010, Strait, et al., 2007, Strait, et al., 2009, Wroe, et al., 2010, Wroe, et al.,
148 2007) and models are frequently based on medical CT scans. However, another challenge of
149 fossils arises because they are often fragmented and invaded by sedimentary matrix that, due
150 to mineralization processes, is undistinguishable, or at least very difficult to distinguish, from
151 bone in scans. This often precludes, for example, segmentation of sedimentary matrix from

152 bone and does not allow fossils to be modelled reliably in terms of their full anatomical
153 complexity. Indeed, given the multiscale organisation of bone, teeth and soft tissues, it is not
154 within the reach of present technology to produce an accurately realistic model. Moreover,
155 increasing model complexity demands higher computational power for solution (Groning, et
156 al., 2012).

157

158 Model simplification in geometry is therefore useful and necessary to overcome these
159 limitations (Fitton, et al., 2015). Assessment of the impact of simplifications typically relies
160 on comparison of variables of interest in subsequent FEA. Thus, researchers commonly focus
161 on stress/strain magnitudes and directions and compare how different modelling decisions
162 impact on those variables (Groning, et al., 2012, Reed, et al., 2011, Strait, et al., 2005,
163 Szwedowski, et al., 2011, Wood, et al., 2011), although bite force has also been used to
164 assess model sensitivity (Fitton, et al., 2012, Sellers and Crompton, 2004). Beyond this, the
165 methods of geometric morphometrics have recently been applied to this task; to compare the
166 deformations of variant models and estimate the impact of such simplifications on results
167 (Fitton, et al., 2015, Fitton, et al., 2012, Godinho, et al., 2017, Toro-Ibacache, et al., 2016).

168

169 The application of GM methods to FEA output is discussed below in more detail, as it is
170 used for the reconstruction of fossils for FEA and in the creation of models of interesting real
171 and hypothetical forms.

172

173 **2. How GM can help in reconstruction**

174 Once the segmentation process is finished, reconstruction of missing anatomical regions
175 begins. This process usually combines imaging software (e.g.
176 Avizo/Amira/Mimics/Geomagic) and GM to approximately restore the original geometry of
177 an incomplete or distorted specimen (Weber, 2015, Weber and Bookstein, 2011). In
178 specimens that preserve one side intact, the most straightforward approach is to use bilateral
179 symmetry (Gunz, et al., 2009). In such cases it is possible to reflect the preserved regions
180 onto the incomplete side and use them to replace the missing areas (Gunz, et al., 2009).
181 However, no skeletal structures are completely symmetric and they present different
182 magnitudes of asymmetry (Quinto-Sánchez, et al., 2015). Thus, reflected regions will not
183 perfectly fit the remaining preserved anatomy. To overcome this mismatch, and account for
184 asymmetry, it is possible to use the thin plate spline (TPS) function to warp the reflected

185 structure onto the remaining preserved anatomy (Gunz, et al., 2009). Even though this is a
186 desirable approach, fossils often lack preserved structures on both sides or along the midline,
187 thus precluding reflection. In these cases reference based reconstruction (Gunz, et al., 2004,
188 Gunz, et al., 2009) should be used. The choice of reference specimen should be considered
189 carefully so as to not bias the reconstruction and it has been suggested that references should
190 be species specific (Gunz, et al., 2009, Senck, et al., 2015, Zollikofer and Ponce de León,
191 2005). Such reconstructions may be statistical or geometric (Gunz, et al., 2004, Gunz, et al.,
192 2009, Neeser, et al., 2009). Statistical reconstruction uses covariances among landmarks in a
193 given sample to predict the location of missing landmarks via multivariate regression (Gunz,
194 et al., 2009, Neeser, et al., 2009). Geometric reconstruction uses the TPS function to estimate
195 the position of the missing landmarks based on known ones (Gunz, et al., 2004, Gunz, et al.,
196 2009). The latter has the advantage of requiring one single specimen, which may be a
197 particular individual or a mean specimen calculated from a given sample using GM (Gunz, et
198 al., 2009) but omits information on intra specific covariations. However, Senck and
199 Coquerelle (2015) show that using mean specimens yields good results when reconstructing
200 large portions of incomplete specimens. Further where sample sizes are limited to one or a
201 few specimens, as with fossils, TPS based warping can be applied, whereas statistical
202 approaches cannot.

203

204 **3. How GM can generate interesting hypothetical forms**

205 Transforming an existing model into a target specimen is of significant value in allowing us
206 to visualise the results of GM analyses. To that end an original specimen may be landmarked
207 densely and then warped into a target that was landmarked similarly (O'Higgins, et al., 2011,
208 Stayton, 2009). Models that represent extremes of morphological variation within a taxon
209 may be created applying a similar approach. Such models can readily be used to simulate
210 mechanical loading and examine the impact of intra-specific morphological variance on
211 mechanical function (Smith, et al., 2015a). One major obstacle to using such an approach is
212 that accurate warping of one specimen into another requires many landmarks and
213 semilandmarks and even then, internal structures such as tooth roots, sinuses and cancellous
214 bone are unlikely to be warped to the form they would have in the target specimen. This is
215 because such internal architecture is very finely detailed and sinuses and cancellous bone
216 architecture are, to great extent, the result of adaptation in the specific individual to habitual
217 loading, this is not accounted for by warping alone. Any errors in warping will therefore

218 likely impact the resulting deformations of the FE model. An alternative is to warp ‘solid’
219 models, ones in which all that is represented is the geometry of the cranial surfaces with the
220 spaces in between infilled with homogenous material. Cancellous bone and sinuses are filled
221 and teeth are not represented as distinct structures, but merely as material with the properties
222 of bone, and with roots merged with the surrounding bone. This is a drastic manoeuvre and a
223 gross simplification. As such, the question arises as to what solid simplified models can tell
224 us?

225

226 Parr et al. (2012) examined the impact of infilling mandibular cavities on the deformations
227 (bending displacements and strain magnitudes frequency) experienced by the mandible of a
228 varanoid lizard during simulated loading. They show that models with infilled cavities
229 deform less than, but generally similarly to, models with preserved cavities. Likewise, Fitton
230 et al. (2015) investigated the effects of simplifying details of internal anatomy
231 (presence/absence of the maxillary sinus) and material properties of teeth in a *Macaca*
232 *fascicularis* cranium, concluding that it does not impact significantly on large scale
233 deformations but it does have localized effects in strain distributions. Toro-Ibacache (2016)
234 addressed the impact of segmentation protocols and of simplifying material properties of a
235 cadaveric human cranium. They concluded that segmentation protocols can have a significant
236 impact on large scale deformations but that simplifying material properties (differentiating
237 trabecular bone from cortical bone vs not differentiating between the two) had little impact on
238 mode of deformation. Thus, if constraints and loads are held constant, solid models behave
239 similarly to much more detailed ones. The key difference emerging from these studies is that
240 the solid models deform less, and so absolute magnitudes of deformation (measured as strains
241 or in terms of changes in size and shape; see below) are not accurately predicted while the
242 mode of deformation (how it deforms) is more consistent. This leads to the realisation that
243 solid models are useful in studies where absolute magnitudes of strains are of no interest but
244 rather, the focus is on mode, how a cranium deforms.

245

246 These findings open up the possibility of carrying out many interesting ‘virtual experiments’
247 by warping or modifying skeletal anatomy to predict the functional role of particular features
248 (O’Higgins, et al., 2011). Strait et al. (2007) applied this virtual experiment approach to infer
249 the relevance of thick palates in Australopiths by experimentally thickening the hard palate of
250 a *Macaca fascicularis* and measure resulting strains. Fitton et al. (2009) reconstructed a
251 specimen of *Australopithecus africanus* (STS 5) and warped the zygomatic region to that of a

252 *Paranthropus boisei* (OH 5) while maintaining the remaining anatomy constant. In both
253 cases, the impact of such modifications was assessed in terms of their impact on stresses and
254 strains in the face.

255

256 **4. How GM can be used to compare FEA results**

257 While stresses and strains from FEA are informative with regard to how skeletal structures
258 bear loads and where they are likely to fail at a localized level (elements or nodes of
259 elements) they do not allow ready assessment of how the model deforms as a whole, for
260 instance, how it bends, twists and undergoes other changes in size and shape. Rather, such
261 modes have to be inferred from strain contour maps based on expertise and knowledge.

262 GM, on the other hand, uses configurations of landmark coordinates and multivariate
263 statistics to assess how specimens differ in form, thereby quantifying morphological
264 differences in size and shape. Thus, it has been proposed that GM can be used to measure and
265 describe global deformations (defined here as changes in size and shape) of models under
266 loading (O'Higgins, et al., 2011, O'Higgins, et al., 2012). This approach differs from GM
267 shape analyses in that size is also simultaneously considered, because loadings change the
268 shape and the size of objects. The basis and application of this approach is described more
269 fully in section 5.3.

270

271 **5. Example Studies**

272 To illustrate how the approaches described above are applied in practice, example studies are
273 presented and reviewed, below.

274

275 **5.1 Reconstruction of crania**

276 We illustrate the application of GM to reconstruction using a CT scan of the cranium of
277 Kabwe 1, which is remarkably well preserved but still presents missing and damaged
278 anatomy due to taphonomic and pathological processes (Schwartz and Tattersall, 2003).
279 Missing anatomical regions include a large portion of the right side of the cranial vault and
280 base (affecting parts of the right temporal, parietal, zygomatic and occipital bone), a small
281 region of the alveolus of the maxilla, teeth and small portions of the orbital cavities (Figure
282 1A). The reconstruction was based on a CT scan (courtesy of Robert Kruszynski, Natural

283 History Museum, London) performed using a Siemens Somatom Plus 4 CT scanner, with
284 voxel size of 0.47 x 0.47 x 0.50 mm and 140 kVp. Reconstruction started with the
285 segmentation of the existing anatomy from the volume. Reconstruction of the left side of the
286 vault followed, and this was later used to restore the large region missing from the right side
287 of the cranium. Lastly, all remaining missing anatomical regions were reconstructed.
288 Segmentation was performed in Avizo 7.0 (Visualization Sciences Group Inc.) and used a
289 variety of approaches. The initial segmentation applied a half maximum height value
290 (HMHV; Spoor et al., 1993) to the whole volume to threshold segment it. Regional
291 thresholds were subsequently calculated and applied to specific anatomical regions as a
292 second step because the HMHV did not segment thin bones. Manual segmentation was also
293 applied for fine details of thin bones that were not picked up by the two previous approaches.
294 Because teeth present clearly different grey values specific thresholds were calculated and
295 applied so as to not overestimate their dimensions. Last, existing sedimentary matrix was
296 removed manually.

297
298 Once the segmentation of existing structures was complete, the large missing region of the
299 right half of the cranium was restored by reflecting the existing contralateral half and fitting
300 (warping) it to the existing structures. This last step used the TPS function and is necessary
301 because crania are not absolutely symmetric. This warping is achieved by placing matching
302 landmarks on the damaged region and reflected fragment and then deforming (warping) the
303 fragment to the cranium using the 'Bookstein' warping function. This resulted in an almost
304 perfect fit between the restored and preserved anatomy, requiring only minimal manual
305 editing. Restoration of the damaged alveolar process of the right hemi-maxilla was also
306 achieved by reflecting the preserved left region. Existing gaps (such as the one present in the
307 orbital surfaces of the maxilla and ethmoid, internal nasal walls, maxilla, occipital bone, left
308 temporal bone, ethmoid bone and vomer) were restored using a combination of manual
309 editing and the software Geomagic Studio 2011 (courtesy of DR W. Sellers, University of
310 Manchester) to interpolate between existing bone edges. The missing posterior region of the
311 occipital bone was reconstructed using the occipital of a modern human cranium, which was
312 manually edited using Geomagic to adjust its morphology. Teeth were preferentially restored
313 by reflecting existing antimeres. When this was not possible portions of teeth from a modern
314 human were used to reconstruct incomplete teeth (final result of reconstruction in Figure 1B).

315
316

317 Figure 1

318

319

320 **5.2 Hypothetical forms**

321 FEA may be applied to any model, whether it represents a real specimen or not. For instance
322 a prior GM analysis may have established the mean form and limits of variation of a
323 landmark configuration taken on a sample of crania. Rather than be interested in how any
324 particular specimens perform, we may be interested in the range of performances represented
325 by the sample. Earlier we noted that solid models, in which internal detail is grossly
326 simplified and filled, provide a reasonable basis for experimental manipulation of FE models
327 to assess specific questions such as the effects of varying palatal thickness or maxillary
328 morphology. This same principle can be extended to whole landmark configurations such as
329 those representing the limits of variation of a sample. By using triplets of thin plate splines to
330 warp whole crania between the mean and these limits of variation hypothetical crania can be
331 created. They do not represent real crania but rather a statistical result from prior
332 morphometric analyses, in this case limits of variation but also, feasibly, through regression
333 or partial least squares (PLS), they could represent forms at the limits of cranial covariation
334 with some interesting ecological or functional variables (e.g. climatic or dietary data,
335 measured bite forces etc.). FEA is then carried out on these hypothetical forms to see how the
336 modes of variation of cranial form identified in the analysis impact performance when the
337 cranium is loaded.

338

339 This warping approach is illustrated here using a simple example; the Kabwe 1 cranium
340 warped into a mean Neanderthal (model 2) using thin plate splines based on classical and
341 sliding semi-landmarks. Classical landmarks (Figure 2, red spheres) of the mean Neanderthal
342 were calculated from 4 Neanderthal crania (Gibraltar 1, Guattari, La Chapelle-aux-Saints, La
343 Ferrassie). The sliding semi-landmarks on the maxilla and brow-ridge (yellow spheres) were
344 calculated from the 4 specimens and the sliding semi-landmarks of the vault and zygoma
345 (light blue spheres) were calculated from the 2 crania in which these structures are almost
346 completely preserved (Guattari and La Ferrassie). In Figure 2, the original model of Kabwe is
347 shown on the left (Figure 2A) and the warped 'mean Neanderthal' on the right (Figure 2B). It
348 is clear that a visually satisfactory result is obtained but of course internal architecture (tooth

349 roots, cortical thicknesses, cavities, sinuses and cancellous bone) will also be warped, not
350 necessarily in such a way that they reasonably represent the average form in Neanderthals.
351 However, by using ‘solid’ models as described above such errors are avoided. The FEA in
352 such a circumstance does not aim to predict and compare actual deformations but rather it
353 provides an answer to a different type of question: how do the differences in external form
354 between these models impact mode and magnitude of deformation?

355 This approach is more limited than we may wish but it is useful in many contexts, for
356 instance in considering how facial retraction vs projection, or brachycephaly vs
357 dolichocephaly, or the mode of form variation predicted by e.g. climate or diet etc. impact on
358 model performance. These are more general questions whose answer does not rest on study
359 of single specimens, but rather on consideration of general modes of variation and their
360 general effects.

361

362

363 Figure 2

364

365

366 **5.3 Application of GM methods to the comparison of FEA results**

367 As noted earlier a third way in which GM methods complement FEA is through comparison
368 of deformations that occur due to loading (O'Higgins, et al., 2011, O'Higgins, et al., 2012).
369 This approach has been applied in several studies (Cox, et al., 2011, Fitton, et al., 2015,
370 Groning, et al., 2012, Groning, et al., 2011a, Holland, 2013, Prôa, 2013, Toro-Ibacache, et al.,
371 2016). Such analyses of deformation rely on assessment of changes in model size and shape,
372 rather than of shape alone as is common in GM studies of organismal variation. This is
373 because as a model is loaded it changes in both size and shape, and it makes no sense to focus
374 on one aspect alone (shape or size). In consequence size and shape are analysed jointly, using
375 rescaled shape coordinates from GPA. The resulting size and shape distances between
376 unloaded and loaded forms describe the magnitudes of deformation and the direction of the
377 vector connecting unloaded and loaded forms in the size and shape space describes the mode
378 of deformation. These vectors can be compared among different load cases applied to the
379 same model or among different models by ignoring the differences in size and shape among
380 unloaded forms and focussing in the vectors connecting unloaded and loaded forms.

381 We illustrate the application of this approach by summarizing a study (Godinho, et al., 2017,
382 Toro-Ibacache, et al., 2016) that examines the impact of simplifications of a cadaveric *Homo*
383 *sapiens* cranium on the resulting modes of deformation predicted by FEA. Specifically, it
384 assesses the impact of simplifications among a three materials model (cortical bone,
385 cancellous bone and teeth; model 3), a two materials (cortical bone and teeth; model 2) and a
386 one material model (everything with material properties of cortical bone; model 1). Thus
387 model 1 is a simple 'solid' model (see above) and model 3 is a much more anatomically
388 accurate model. The models are loaded to simulate a bite on the first molar, although the
389 applied forces are not physiological, rather they replicate the loading of an accompanying
390 validation study to facilitate comparison with that in ongoing work.

391 The results in terms of strain contour plots (not shown), suggest that variations among models
392 generally impact on magnitudes of strains but not so much on the distribution of regions of
393 high and low strain throughout the model. The GM analysis of deformations complements
394 these findings. Size and shape distances are calculated by multiplying the shape coordinates
395 (from GPA) of each specimen by that specimen's original centroid size. This results in the
396 specimens being represented by points in a (size and shape) space that can be thought of as
397 the space of GPA aligned coordinates (Slice 2001), an approximation of Kendall's shape
398 space, with size as an additional dimension. The vector of centroid size (the additional
399 dimension) at any point on the manifold can be visualised as passing radially from the
400 centroid of the manifold of this space (zero size), through the manifold (centroid size = 1) and
401 beyond to infinity (infinite size). When centroid size is 1, the objects lie on the manifold of
402 the space of GPA aligned coordinates (Figure 3). The resulting space differs from the classic
403 size and shape space (Dryden and Mardia, 1998) that results from translating and rotating, but
404 not scaling landmark configurations. In particular, the rotations of configurations with respect
405 to each other differ because size influences rotation. In consequence the estimates of mean
406 size and shape (the size and shape variables; translated and rotated coordinates) obtained by
407 these two approaches, the resulting covariance matrix, and so PCA, also differ. However in
408 the application to FEA, where deformations are extremely small, the resulting size and shape
409 differences are negligible. Either space could be used, with almost no difference in results,
410 but the approach we adopt is useful in understanding how shape analysis and size and shape
411 analysis are related (Figure 3). Thus, simply making the model stiffer or less stiff (material
412 properties) or applying the same force vectors but varying their magnitudes results in greater
413 or less deformation; the vectors connecting unloaded and loaded models simply scale directly
414 with force or inversely with Young's modulus (a measure of stiffness). Deformations (size

415 and shape distances) also scale inversely with model centroid size if loads, geometry and
416 material properties are held constant. In contrast Procrustes distances scale inversely with the
417 square of centroid size. Figure 3 illustrates these scaling relationships with centroid size.
418 Thus if we take the shape of the black point (a; on the GPA hemisphere, centroid size =1;
419 Fig. 3) to be the unloaded form and the grey point (b) as the shape of the loaded form, the
420 distance between them represents the deformation in shape and approximates Procrustes
421 distance when variations are small. If size also differs due to loading, then the loaded form
422 does not lie on the hemisphere but is above (grey point, c) or below it depending on if it
423 increased or decreased in centroid size. The distance (a-c) between loaded and unloaded
424 forms is the size and shape distance and is a measure of deformation (change in size and
425 shape with loading).

426

427 If the same forces and same material properties apply but the unloaded form is larger (black
428 point, d, on the outer semicircle representing the GPA hemisphere with centroid size >1 in
429 Fig 3) the resulting deformation in size and shape is less (distance d-f; which in this diagram
430 is shown larger than in reality to facilitate visualisation). The physics dictate that the size and
431 shape distances (deformations) between unloaded and loaded objects scale inversely with
432 centroid sizes of the unloaded objects; bigger forms deform less under the same load.
433 However, shape change due to loading (Procrustes distance as opposed to size and shape
434 distance) scales inversely with the *square* of the centroid size of the unloaded object. Thus,
435 scaling the unloaded large object, d, to centroid size 1, results in it overlying point a, the
436 unloaded object with centroid size 1 (these are identical in shape but differ only in size).
437 Scaling the loaded large object, f, to centroid size 1 projects it along a radius (dashed line in
438 Fig. 3) through point e to an intersection, g, with the arc of the GPA hemisphere. As a result
439 of this scaling, the ratio of Procrustes distances (a-b)/(a-g) is the inverse of the ratio of the
440 squares of centroid sizes of the unloaded forms, a and d.

441

442 These scaling ratios are important because they allow us to account (at least approximately)
443 for differences in size when comparing deformations predicted by FEA among similar objects
444 using geometric morphometric methods. Such scaling is inevitably an approximation unless
445 the objects whose deformations are being compared are the same shape, differing only in
446 size. As shapes become more different, it makes less sense to compare deformations and the
447 degree of approximation in scaling increases.

448

449 Figure 3

450

451

452 Principal components analysis using the covariance matrix among size and shape variables
453 can be used to visualise and compare deformations. Figure 4 presents the first two principal
454 components from the sensitivity study we conducted on a *Homo sapiens* of model
455 simplification with regard to segmentation and allocation of material properties. These
456 account for some 99% of the total variance and so fairly represent the results. Included in the
457 analysis are the unloaded model and the three variants of model segmentation (model 1,
458 whole model as cortical bone = 17 GPa; model 2, bone = 17 GPa and teeth = 50 GPa; model
459 3, cortical bone = 17GPa, cancellous bone = 56 MPa, teeth = 50 GPa; all materials allocated a
460 Poisson's ratio of 0.3) after loading in a simulated first molar bite. Model 3 is also loaded in a
461 simulated incisor bite. This allows the effects of simplification to be compared against the
462 effect of varying bite point. The molar bites cluster away from the incisor bite, indicating
463 they are more similar in mode of deformation. The modes of variation are represented by the
464 vectors connecting unloaded and loaded models. They are visualised by the inset warped
465 surface models and transformation grids, computed using thin plate splines and magnified
466 500 times to facilitate interpretation. Models 2 and 1 overlie each other and so are represented
467 by a single point. This implies that representing dental roots as cortical bone has little effect.
468 Modes of deformation differ greatly between incisor and molar bites and consist mainly of
469 upwards deflection of the anterior maxilla in the former and of the lateral maxilla in the latter.
470 With regard to the molar bites, simplification has its greatest impact when cancellous bone is
471 allocated the material properties of cortical, effectively making a 'solid' model. The effect is
472 to reduce the degree of deformation as is reflected in the shorter vector connecting models 1
473 and 2 with the unloaded than that connecting model 3. Similarly the degree of deformation
474 evident in the inset warpings is reduced. There is a difference in mode of deformation as
475 evidenced by the angle between these vectors but the difference in mode is less obvious in
476 comparing the inset warping for models 2 and 3 with that for model 1.

477 The impact of simplification on mode of deformation is small compared to the large
478 difference between molar and incisor bites.

479

480

481 Figure 4

482

483

484 This simple analysis can be extended to more complex and interesting questions concerning
485 multiple variants of models and to the comparison of deformations among models (O'Higgins
486 and Milne, 2013) by focusing on differences among vectors of deformation rather than
487 differences among unloaded forms. This application of GM is particular useful in relation to
488 FEA sensitivity studies providing an easily visible and quantifiable approach to the
489 assessment of model “error” and sensitivity. Comparisons can be made within and between
490 models to assess whether differences in performance due to modelling assumptions are
491 drowning out any meaningful biological signals.

492

493 **6. Discussion**

494 The last three decades have seen an explosion of advances in techniques pertinent to the
495 study of skeletal change through time. Morphometrics underwent a revolution (Adams, et al.,
496 2004, Rohlf and Marcus, 1993) beginning in the late 1970's (Bookstein, 1978) and gathering
497 pace through the next three decades. This, in common with the tools for high resolution
498 imaging, visualisation and manipulation of images, took great advantage of the advances in
499 computing that occurred over the same period. These same advances in computational power
500 led to the development of increasingly sophisticated software tools for FEA, to simulate and
501 predict the effects of loadings on structures.

502

503 All of these tools are in common use today in the field of Archaeology, in particular they
504 have been driven by work on fossil material, but increasingly they are applied to more recent
505 skeletal finds, archaeobotany (García-Granero, et al., 2016, Ros, et al., 2014), zooarchaeology
506 (Cucchi, et al., 2011, Evin, et al., 2013, Owen, et al., 2014) and to material culture such as
507 ancient architecture (Levy and Dawson, 2009), stone tools (Buchanan and Collard, 2010,
508 Buchanan, et al., 2011, Okumura and Araujo, 2014), and pottery (Hein, et al., 2008,
509 Kilikoglou and Vekinis, 2002, Wilczek, et al., 2014). As these tools have become more
510 commonly applied, useful ways of combining them have come to the fore. Thus, GM
511 methods combined with tools for imaging and image manipulation can play an important role
512 in the reconstruction of skeletal material, as illustrated by the first example we present in this
513 paper.

514

515 Reconstruction provides data for morphometric analyses and GM has proven powerful in this
516 domain. Beyond the fact that these methods provide approaches that are statistically robust
517 and well understood, GM's great advantage for many workers lies in the ability to visualise
518 the results of statistical analyses as warpings of the mean form. These visualisations close the
519 loop between measurement, statistics and interpretation of results in terms of changes in size
520 and shape. They also can be used to produce 3D models of the results of statistical analyses
521 such as mean forms or forms representing extremes of variation or extremes of interesting
522 modes of variation, such as the limits of regressions of form on ecological, behavioural and
523 functional data. In turn, such forms are potentially interesting targets for FEA. For instance,
524 the results of a study of how cranial form covaries with the toughness of diet might be
525 actualised as a pair of 3D surfaces representing crania at the limits of the regression; those
526 suited to tough and those suited to less tough diets. These can be submitted to FEA to explore
527 how each responds to loading and, in this way, link modes of morphological variation to load
528 resistance. This kind of analysis provides a very direct way of exploring how form and
529 function interact.

530

531 These kinds of studies depend critically on the validity of FEA modelling and on how
532 sensitive such modelling is to errors in model building and loading. Validity is assessed by
533 comparing predicted strains with directly measured, real strains. Sensitivity, on the other
534 hand is assessed by varying model parameters to replicate likely errors and comparing results
535 among (often many) variant models as in the example we provide earlier. In this endeavour,
536 GM has been usefully combined with FEA.

537

538 Size and shape analysis allows ready understanding of the effects of different model building
539 decisions in terms of how the models deform and how they differ in deformation. It leads to
540 statements about changes in form such as how a skull twists or bends under loading. If,
541 instead of landmarks the coordinates of all nodes of the finite element mesh are submitted to
542 analysis, strains can be computed from the coordinates of the unloaded and loaded meshes.

543 On the other hand the concentrations of stresses or strains in localised regions are useful
544 predictors of failure and while the overall distribution of strains can be used to infer global
545 modes of deformation this requires simultaneous interpretation of one contour map for each
546 principal strain (2 in 2D analyses and 3 in 3D). Thus the approaches can be considered
547 complementary. GM analyses inform with regard to how loading deforms an object, in terms

548 of changes in size and shape. On the other hand, stresses and strains inform with regard to the
549 likelihood of failure in particular anatomical regions and how distributions of high and low
550 strains may eventually relate to (re)modelling fields. Each can be used to infer the other, thus
551 GM analyses that use the coordinates of the nodes of an FE mesh result in visualisations of
552 deformations of that mesh and strains can be computed and displayed in these meshes, while
553 strains can be used to infer global degrees and modes of deformation. It should be noted that
554 the metric of the GM analysis, the Procrustes size and shape distance relates to changes in
555 size and shape, not the risk of failure. It differs from metrics derived from strains. These
556 describe different aspects of deformation that are complementary, but not coincident, in
557 interpreting FEA results.

558

559 Beyond sensitivity analyses, GM methods have been extended to the task of comparing
560 deformations among different specimens modelled and loaded in equivalent ways (Milne and
561 O'Higgins, 2012, O'Higgins and Milne, 2013). In this case the analysis focuses on differences
562 in vectors of deformation rather than the differences between unloaded forms. This is
563 achieved by computing deformations as differences between registered loaded and unloaded
564 forms. They can be visualised by adding these vectors to a convenient unloaded form such as
565 the mean of all unloaded specimens. Beyond comparisons of deformation, it is also possible
566 to use GM approaches to assess the association between deformation under loading and other
567 interesting factors such as skeletal form or ecological variables through regression of PLS
568 analyses. This has not yet been much exploited in the literature but is likely to increasingly be
569 taken up as a useful approach to the interpretation of the biological significance of differences
570 in modes and magnitudes of variation. Differences among models in size, applied forces and
571 material properties can be taken into account by 'correcting' the magnitudes of deformations
572 according to the known scaling relationships described above.

573

574 The application of GM methods in conjunction with FEA is as yet in its infancy. There are
575 clear roles for GM methods in reconstruction, the production of models with modified
576 geometry to explore how form and function interact and in comparing the results of FEAs
577 among models and load cases. Each of these approaches has potential benefits and pitfalls
578 and, in time, with increasing numbers of studies applying these methods we will better
579 understand where they are applicable and where not. At present these combined GM/FEA
580 approaches are still fairly novel and some years of methodological development can be
581 anticipated.

582

583 **Acknowledgements**

584 We are grateful for support provided to R. M. Godinho by the Portuguese Foundation for
585 Science and Technology (PhD funding reference: SFRH/BD/76375/2011) and to Fred
586 Bookstein, Dennis Slice, Ian Dryden and Chris Klingenberg for their feedback and critiques
587 of particularly the GM analysis of deformations resulting from FEA, provided on many
588 occasions over recent years.

589

590 **References**

591

592 Adams, D.C., Rohlf, F.J., Slice, D.E., 2004. Geometric morphometrics: ten years of progress
593 following the 'revolution', Italian Journal of Zoology 71, 5-16.

594 Antón, S.C., 1990. Neandertals and the anterior dental loading hypothesis: a biomechanical
595 evaluation of bite force production, Kroeber Anthropological Society Papers 71-72, 67-76.

596 Attard, M.R.G., Parr, W.C.H., Wilson, L.A.B., Archer, M., Hand, S.J., Rogers, T.L., Wroe,
597 S., 2014. Virtual Reconstruction and Prey Size Preference in the Mid Cenozoic Thylacinid,
598 *Nimbacinus dicksoni* (Thylacinidae, Marsupialia), Plos One 9, e93088.

599 Bates, K.T., Falkingham, P.L., 2012. Estimating maximum bite performance in
600 Tyrannosaurus rex using multi-body dynamics, Biol Letters 8, 660-664.

601 Bookstein, F., 1978. The Measurement of Biological Shape and Shape Change, Springer,
602 Berlin.

603 Braun, S., Bantleon, H.-P., Hnat, W.P., Freudenthaler, J.W., Marcotte, M.R., Johnson, B.E.,
604 1995. A study of bite force, part 1: Relationship to various physical characteristics, The
605 Angle Orthodontist 65, 367-372.

606 Bright, J.A., Groning, F., 2011. Strain Accommodation in the Zygomatic Arch of the Pig: A
607 Validation Study Using Digital Speckle Pattern Interferometry and Finite Element Analysis,
608 Journal of Morphology 272, 1388-1398.

609 Buchanan, B., Collard, M., 2010. A geometric morphometrics-based assessment of blade
610 shape differences among Paleoindian projectile point types from western North America, J
611 Archaeol Sci 37, 350-359.

- 612 Buchanan, B., Collard, M., Hamilton, M.J., O'Brien, M.J., 2011. Points and prey: a
613 quantitative test of the hypothesis that prey size influences early Paleoindian projectile point
614 form, *J Archaeol Sci* 38, 852-864.
- 615 Cox, P.G., Fagan, M.J., Rayfield, E.J., Jeffery, N., 2011. Finite element modelling of squirrel,
616 guinea pig and rat skulls: using geometric morphometrics to assess sensitivity, *J Anat* 219,
617 696-709.
- 618 Cox, P.G., Rayfield, E.J., Fagan, M.J., Herrel, A., Pataky, T.C., Jeffery, N., 2012. Functional
619 Evolution of the Feeding System in Rodents, *Plos One* 7.
- 620 Cox, P.G., Rinderknecht, A., Blanco, R.E., 2015. Predicting bite force and cranial
621 biomechanics in the largest fossil rodent using finite element analysis, *J Anat* 226, 215-223.
- 622 Cucchi, T., Hulme-Beaman, A., Yuan, J., Dobney, K., 2011. Early Neolithic pig
623 domestication at Jiahu, Henan Province, China: clues from molar shape analyses using
624 geometric morphometric approaches, *J Archaeol Sci* 38, 11-22.
- 625 Curtis, N., Kupczik, K., O'Higgins, P., Moazen, M., Fagan, M., 2008. Predicting skull
626 loading: Applying multibody dynamics analysis to a macaque skull, *Anat Rec* 291, 491-501.
- 627 Degrange, F.J., Tambussi, C.P., Moreno, K., Witmer, L.M., Wroe, S., 2010. Mechanical
628 Analysis of Feeding Behavior in the Extinct "Terror Bird" *Andalgalornis steulleti*
629 (Gruiformes: Phorusrhacidae), *Plos One* 5, e11856.
- 630 Demes, B., 1987. Another Look at an Old Face - Biomechanics of the Neandertal Facial
631 Skeleton Reconsidered, *J Hum Evol* 16, 297-303.
- 632 Demes, B., Creel, N., 1988. Bite Force, Diet, and Cranial Morphology of Fossil Hominids, *J*
633 *Hum Evol* 17, 657-670.
- 634 Dryden, I.L., Mardia, K.V., 1998. *Statistical Shape Analysis*, Wiley-Blackwell.

635 Eng, C.M., Lieberman, D.E., Zink, K.D., Peters, M.A., 2013. Bite force and occlusal stress
636 production in hominin evolution, *Am J Phys Anthropol* 151, 544-557.

637 Evin, A., Cucchi, T., Cardini, A., Strand Vidarsdottir, U., Larson, G., Dobney, K., 2013. The
638 long and winding road: identifying pig domestication through molar size and shape, *J*
639 *Archaeol Sci* 40, 735-743.

640 Fitton, L., Groening, F., Cobb, S., Fagan, M., O'Higgins, P., 2009. Biomechanical
641 Significance of Morphological Variation between the Gracile *Australopithecus Africanus*
642 (STS5) and Robust *Australopithecus Boisei* (OH5), *J Vertebr Paleontol* 29, 96a-96a.

643 Fitton, L.C., Prôa, M., Rowland, C., Toro-Ibacache, V., O'Higgins, P., 2015. The Impact of
644 Simplifications on the Performance of a Finite Element Model of a *Macaca fascicularis*
645 Cranium, *The Anatomical Record* 298, 107-121.

646 Fitton, L.C., Shi, J.F., Fagan, M.J., O'Higgins, P., 2012. Masticatory loadings and cranial
647 deformation in *Macaca fascicularis*: a finite element analysis sensitivity study, *J Anat* 221,
648 55-68.

649 Gans, C., de Vree, F., 1987. Functional bases of fiber length and angulation in muscle,
650 *Journal of Morphology* 192, 63-85.

651 García-Granero, J.J., Arias-Martorell, J., Madella, M., Lancelotti, C., 2016. Geometric
652 morphometric analysis of *Setaria italica* (L.) P. Beauv. (foxtail millet) and *Brachiaria ramosa*
653 (L.) Stapf. (browntop millet) and its implications for understanding the biogeography of small
654 millets, *Vegetation History and Archaeobotany* 25, 303-310.

655 Godinho, R.M., O'Higgins, P., 2017. Virtual reconstruction of cranial remains: the H.
656 Heidelbergensis, Kabwe 1 fossil, in: Thompson, T., Errickson, D. (Eds.), *Human remains -*
657 *Another dimension: the application of 3D imaging in funerary context*, Elsevier, London, pp.
658 135-147.

659 Godinho, R.M., Toro-Ibacache, V., Fitton, L.C., O'Higgins, P., 2017. Finite element analysis
660 of the cranium: Validity, sensitivity and future directions, *Cr Palevol* 16, 600-612.

661 Groning, F., Fagan, M., O'Higgins, P., 2012. Modeling the Human Mandible Under
662 Masticatory Loads: Which Input Variables are Important?, *Anat Rec* 295, 853-863.

663 Groning, F., Fagan, M.J., O'Higgins, P., 2011a. The effects of the periodontal ligament on
664 mandibular stiffness: a study combining finite element analysis and geometric
665 morphometrics, *J Biomech* 44, 1304-1312.

666 Groning, F., Liu, J., Fagan, M.J., O'Higgins, P., 2009. Validating a voxel-based finite element
667 model of a human mandible using digital speckle pattern interferometry, *J Biomech* 42, 1224-
668 1229.

669 Groning, F., Liu, J., Fagan, M.J., O'Higgins, P., 2011b. Why Do Humans Have Chins?
670 Testing the Mechanical Significance of Modern Human Symphyseal Morphology With Finite
671 Element Analysis, *Am J Phys Anthropol* 144, 593-606.

672 Gunz, P., Mitteroecker, P., Bookstein, F., Weber, G., 2004. Computer-aided reconstruction of
673 incomplete human crania using statistical and geometrical estimation methods, *Computer*
674 *Applications and Quantitative Methods in Archaeology*, Archaeopress, pp. 92–94.

675 Gunz, P., Mitteroecker, P., Neubauer, S., Weber, G.W., Bookstein, F.L., 2009. Principles for
676 the virtual reconstruction of hominin crania, *J Hum Evol* 57, 48-62.

677 Hein, A., Georgopoulou, V., Nodarou, E., Kilikoglou, V., 2008. Koan amphorae from
678 Halasarna – investigations in a Hellenistic amphora production centre, *J Archaeol Sci* 35,
679 1049-1061.

680 Holland, M., 2013. The effect of the inclusion of the periodontal ligament upon the stiffness
681 of a human cranial finite element model: a validated sensitivity study, HYMS, University of
682 York, York.

683 Josephson, R.K., 1975. Extensive and intensive factors determining the performance of
684 striated muscle, *J Exp Zool* 194, 135-153.

685 Kikuchi, M., Koriath, T.W.P., Hannam, A.G., 1997. The Association Among Occlusal
686 Contacts, Clenching Effort, and Bite Force Distribution in Man, *J Dent Res* 76, 1316-1325.

687 Kilikoglou, V., Vekinis, G., 2002. Failure Prediction and Function Determination of
688 Archaeological Pottery by Finite Element Analysis, *J Archaeol Sci* 29, 1317-1325.

689 Kupczik, K., Dobson, C.A., Fagan, M.J., Crompton, R.H., Oxnard, C.E., O'Higgins, P., 2007.
690 Assessing mechanical function of the zygomatic region in macaques: validation and
691 sensitivity testing of finite element models, *J Anat* 210, 41-53.

692 Ledogar, J.A., Smith, A.L., Benazzi, S., Weber, G.W., Spencer, M.A., Carlson, K.B.,
693 McNulty, K.P., Dechow, P.C., Grosse, I.R., Ross, C.F., Richmond, B.G., Wright, B.W.,
694 Wang, Q., Byron, C., Carlson, K.J., de Ruiter, D.J., Berger, L.R., Tamvada, K., Pryor, L.C.,
695 Berthaume, M.A., Strait, D.S., 2016. Mechanical evidence that *Australopithecus sediba* was
696 limited in its ability to eat hard foods, *Nat Commun* 7.

697 Levy, R., Dawson, P., 2009. Using finite element methods to analyze ancient architecture: an
698 example from the North American Arctic, *J Archaeol Sci* 36, 2298-2307.

699 Lieberman, D., 2011. *The Evolution of the Human Head*, Harvard University Press,
700 Cambridge.

701 McCormack, S.W., Witzel, U., Watson, P.J., Fagan, M.J., Gröning, F., 2014. The
702 Biomechanical Function of Periodontal Ligament Fibres in Orthodontic Tooth Movement,
703 *Plos One* 9, e102387.

704 Milne, N., O'Higgins, P., 2012. Scaling of form and function in the xenarthran femur: a 100-
705 fold increase in body mass is mitigated by repositioning of the third trochanter, *P Roy Soc B-*
706 *Biol Sci* 279, 3449-3456.

707 Neeser, R., Ackermann, R.R., Gain, J., 2009. Comparing the accuracy and precision of three
708 techniques used for estimating missing landmarks when reconstructing fossil hominin crania,
709 *Am J Phys Anthropol* 140, 1-18.

710 O'Connor, C.F., Franciscus, R.G., Holton, N.E., 2005. Bite force production capability and
711 efficiency in neandertals and modern humans, *Am J Phys Anthropol* 127, 129-151.

712 O'Higgins, P., Cobb, S.N., Fitton, L.C., Groning, F., Phillips, R., Liu, J., Fagan, M.J., 2011.
713 Combining geometric morphometrics and functional simulation: an emerging toolkit for
714 virtual functional analyses, *J Anat* 218, 3-15.

715 O'Higgins, P., Fitton, L.C., Phillips, R., Shi, J.F., Liu, J., Groning, F., Cobb, S.N., Fagan,
716 M.J., 2012. Virtual Functional Morphology: Novel Approaches to the Study of Craniofacial
717 Form and Function, *Evol Biol* 39, 521-535.

718 O'Higgins, P., Milne, N., 2013. Applying geometric morphometrics to compare changes in
719 size and shape arising from finite elements analyses, *Hystrix, the Italian Journal of*
720 *Mammalogy* 24, 7.

721 Okumura, M., Araujo, A.G.M., 2014. Long-term cultural stability in hunter-gatherers: a case
722 study using traditional and geometric morphometric analysis of lithic stemmed bifacial points
723 from Southern Brazil, *J Archaeol Sci* 45, 59-71.

724 Oldfield, C.C., McHenry, C.R., Clausen, P.D., Chamoli, U., Parr, W.C.H., Stynder, D.D.,
725 Wroe, S., 2012. Finite element analysis of ursid cranial mechanics and the prediction of
726 feeding behaviour in the extinct giant *Agriotherium africanum*, *J Zool* 286, 171-171.

727 Owen, J., Dobney, K., Evin, A., Cucchi, T., Larson, G., Strand Vidarsdottir, U., 2014. The
728 zooarchaeological application of quantifying cranial shape differences in wild boar and
729 domestic pigs (*Sus scrofa*) using 3D geometric morphometrics, *J Archaeol Sci* 43, 159-167.

730 Paphangkorakit, J., Osborn, J.W., 1997. Effect of Jaw Opening on the Direction and
731 Magnitude of Human Incisal Bite Forces, *J Dent Res* 76, 561-567.

732 Parr, W.C.H., Chamoli, U., Jones, A., Walsh, W.R., Wroe, S., 2013. Finite element micro-
733 modelling of a human ankle bone reveals the importance of the trabecular network to
734 mechanical performance: New methods for the generation and comparison of 3D models, *J*
735 *Biomech* 46, 200-205.

736 Parr, W.C.H., Wroe, S., Chamoli, U., Richards, H.S., McCurry, M.R., Clausen, P.D.,
737 McHenry, C., 2012. Toward integration of geometric morphometrics and computational
738 biomechanics: New methods for 3D virtual reconstruction and quantitative analysis of Finite
739 Element Models, *J Theor Biol* 301, 1-14.

740 Prôa, M., 2013. Cranial Form Evolution and Functional Adaptations to Diet among
741 Papionins: A Comparative Study combining Quantitative Genetics, Geometric
742 Morphometrics, and Finite Element Analysis, Hull York Medical School, University of York,
743 York.

744 Quinto-Sánchez, M., Adhikari, K., Acuña-Alonzo, V., Cintas, C., Silva de Cerqueira, C.C.,
745 Ramallo, V., Castillo, L., Farrera, A., Jaramillo, C., Arias, W., Fuentes, M., Everardo, P., de
746 Avila, F., Gomez-Valdés, J., Hünemeier, T., Gibbon, S., Gallo, C., Poletti, G., Rosique, J.,
747 Bortolini, M.C., Canizales-Quinteros, S., Rothhammer, F., Bedoya, G., Ruiz-Linares, A.,
748 González-José, R., 2015. Facial asymmetry and genetic ancestry in Latin American admixed
749 populations, *Am J Phys Anthropol*, n/a-n/a.

750 Rak, Y., 1983. The Australopithecine Face, in: Rak, Y. (Ed.), *The Australopithecine Face*,
751 Academic Press, p. 1.

752 Rak, Y., 1986. The Neanderthal - a New Look at an Old Face, *J Hum Evol* 15, 151-164.

753 Rayfield, E.J., 2005. Aspects of comparative cranial mechanics in the theropod dinosaurs
754 *Coelophysis*, *Allosaurus* and *Tyrannosaurus*, *Zool J Linn Soc-Lond* 144, 309-316.

755 Rayfield, E.J., 2007. Finite element analysis and understanding the biomechanics and
756 evolution of living and fossil organisms, *Annu Rev Earth Pl Sc* 35, 541-576.

757 Rayfield, E.J., Norman, D.B., Horner, C.C., Horner, J.R., Smith, P.M., Thomason, J.J.,
758 Upchurch, P., 2001. Cranial design and function in a large theropod dinosaur, *Nature* 409,
759 1033-1037.

760 Reed, D.A., Porro, L.B., Iriarte-Diaz, J., Lemberg, J.B., Holliday, C.M., Anapol, F., Ross,
761 C.F., 2011. The impact of bone and suture material properties on mandibular function in
762 Alligator mississippiensis: testing theoretical phenotypes with finite element analysis, *J Anat*
763 218, 59-74.

764 Rohlf, F.J., Marcus, L.F., 1993. A revolution in morphometrics, *Trends Ecol Evol* 8, 129-
765 132.

766 Ros, J., Evin, A., Bouby, L., Ruas, M.-P., 2014. Geometric morphometric analysis of grain
767 shape and the identification of two-rowed barley (*Hordeum vulgare* subsp. *distichum* L.) in
768 southern France, *J Archaeol Sci* 41, 568-575.

769 Ross, C.F., 2005. Finite element analysis in vertebrate biomechanics, *Anat Rec Part A* 283A,
770 253-258.

771 Schwartz, J.H., Tattersall, I., 2003. *The Human Fossil Record - Craniodental Morphology of*
772 *Genus Homo*, Wiley-Liss, USA.

773 Sellers, W.I., Crompton, R.H., 2004. Using sensitivity analysis to validate the predictions of a
774 biomechanical model of bite forces, *Ann Anat* 186, 89-95.

775 Senck, S., Bookstein, F.L., Benazzi, S., Kastner, J., Weber, G.W., 2015. Virtual
776 Reconstruction of Modern and Fossil Hominoid Crania: Consequences of Reference Sample
777 Choice, *The Anatomical Record* 298, 827-841.

778 Senck, S., Coquerelle, M., 2015. Morphological Integration and Variation in Facial
779 Orientation in *Pongo pygmaeus pygmaeus*: A Geometric Morphometric Approach via Partial
780 Least Squares, *Int J Primatol* 36, 489-512.

781 Shi, J.F., Curtis, N., Fitton, L.C., O'Higgins, P., Fagan, M.J., 2012. Developing a
782 musculoskeletal model of the primate skull: Predicting muscle activations, bite force, and
783 joint reaction forces using multibody dynamics analysis and advanced optimisation methods,
784 *J Theor Biol* 310, 21-30.

785 Sinn, D.P., DeAssis, E.A., Throckmorton, G.S., 1996. Mandibular excursions and maximum
786 bite forces in patients with temporomandibular joint disorders, *J Oral Maxil Surg* 54, 671-
787 679.

788 Slice, D.E., 2001. Landmark coordinates aligned by Procrustes analysis do not lie in
789 Kendall's shape space. *Systematic biology*, 50(1), 141-149.

790 Slice, D.E., Chalk, J., Smith, A.L., Smith, L.C., Wood, S., Berthaume, M., Benazzi, S.,
791 Dzialo, C., Tamvada, K., Ledogar, J.A., 2013. Viewpoints: Diet and dietary adaptations in
792 early hominins: The hard food perspective, *Am J Phys Anthropol* 151, 339-355.

793 Smith, A.L., Benazzi, S., Ledogar, J.A., Tamvada, K., Pryor Smith, L.C., Weber, G.W.,
794 Spencer, M.A., Dechow, P.C., Grosse, I.R., Ross, C.F., Richmond, B.G., Wright, B.W.,
795 Wang, Q., Byron, C., Slice, D.E., Strait, D.S., 2015a. Biomechanical Implications of
796 Intraspecific Shape Variation in Chimpanzee Crania: Moving Toward an Integration of
797 Geometric Morphometrics and Finite Element Analysis, *The Anatomical Record* 298, 122-
798 144.

799 Smith, A.L., Benazzi, S., Ledogar, J.A., Tamvada, K., Pryor Smith, L.C., Weber, G.W.,
800 Spencer, M.A., Lucas, P.W., Michael, S., Shekeban, A., Al-Fadhalah, K., Almusallam, A.S.,
801 Dechow, P.C., Grosse, I.R., Ross, C.F., Madden, R.H., Richmond, B.G., Wright, B.W.,
802 Wang, Q., Byron, C., Slice, D.E., Wood, S., Dzialo, C., Berthaume, M.A., van Casteren, A.,
803 Strait, D.S., 2015b. The Feeding Biomechanics and Dietary Ecology of *Paranthropus boisei*,
804 *The Anatomical Record* 298, 145-167.

805 Stayton, C.T., 2009. Application of thin-plate-spline transformations to finite element
806 models, or, how to turn a bog turtle into a spotted turtle to analyze both, *Evolution* 63, 1348-
807 1355.

808 Strait, D.S., Constantino, P., Lucas, P.W., Richmond, B.G., Spencer, M.A., Dechow, P.C.,
809 Ross, C.F., Grosse, I.R., Wright, B.W., Wood, B.A., Weber, G.W., Wang, Q., Byron, C.,

810 Strait, D.S., Grosse, I.R., Dechow, P.C., Smith, A.L., Wang, Q., Weber, G.W., Neubauer, S.,
811 Slice, D.E., Chalk, J., Richmond, B.G., Lucas, P.W., Spencer, M.A., Schrein, C., Wright,
812 B.W., Byfton, C., Ross, C.F., 2010. The Structural Rigidity of the Cranium of
813 *Australopithecus africanus*: Implications for Diet, Dietary Adaptations, and the Allometry of
814 Feeding Biomechanics, *Anat Rec* 293, 583-593.

815 Strait, D.S., Richmond, B.G., Spencer, M.A., Ross, C.F., Dechow, P.C., Wood, B.A., 2007.
816 Masticatory biomechanics and its relevance to early hominid phylogeny: An examination of
817 palatal thickness using finite-element analysis, *J Hum Evol* 52, 585-599.

818 Strait, D.S., Wang, Q., Dechow, P.C., Ross, C.F., Richmond, B.G., Spencer, M.A., Patel,
819 B.A., 2005. Modeling elastic properties in finite element analysis: How much precision is
820 needed to produce an accurate model?, *Anat Rec Part A* 283A, 275-287.

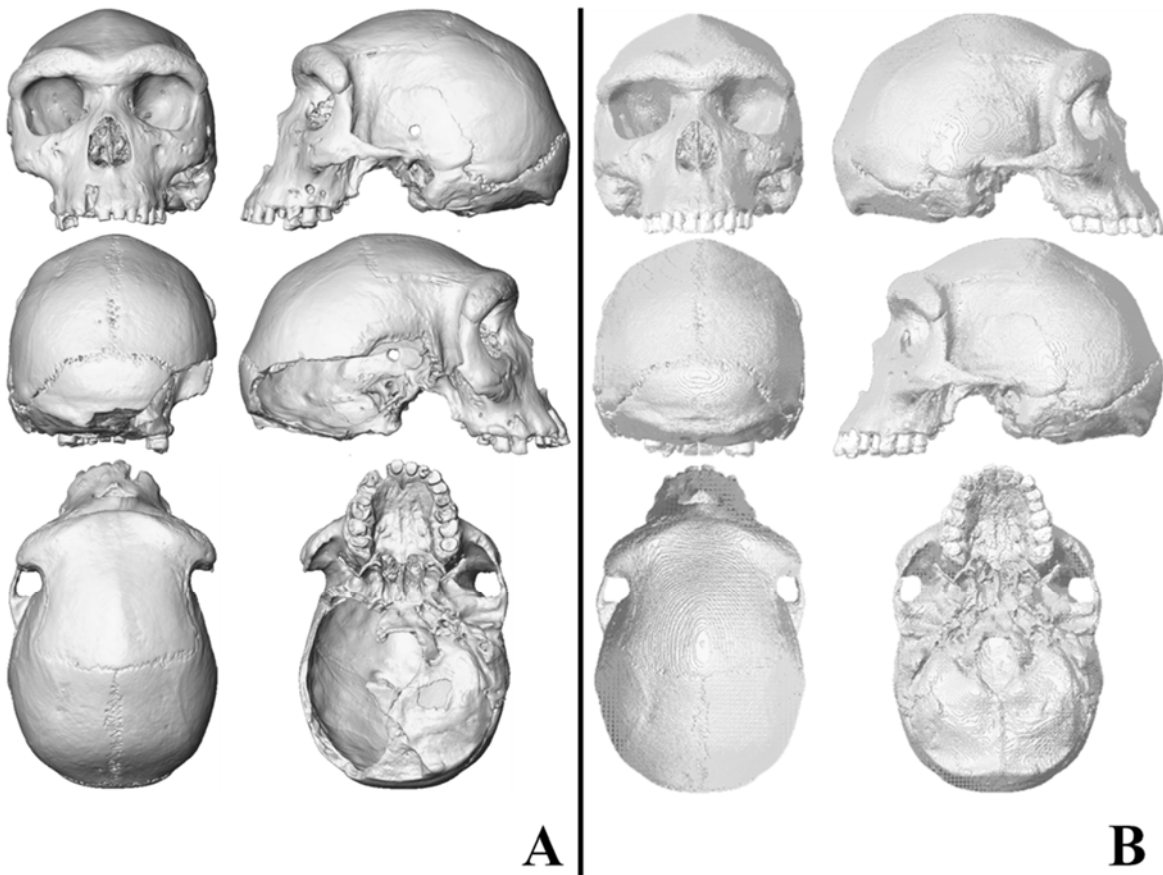
821 Strait, D.S., Weber, G.W., Neubauer, S., Chalk, J., Richmond, B.G., Lucas, P.W., Spencer,
822 M.A., Schrein, C., Dechow, P.C., Ross, C.F., Grosse, I.R., Wright, B.W., Constantino, P.,
823 Wood, B.A., Lawn, B., Hylander, W.L., Wang, Q., Byron, C., Slice, D.E., Smith, A.L., 2009.
824 The feeding biomechanics and dietary ecology of *Australopithecus africanus*, *P Natl Acad*
825 *Sci USA* 106, 2124-2129.

826 Szwedowski, T.D., Fialkov, J., Whyne, C.M., 2011. Sensitivity analysis of a validated
827 subject-specific finite element model of the human craniofacial skeleton, *P I Mech Eng H*
828 225, 58-67.

- 829 Toro-Ibacache, V., Fitton, L.C., Fagan, M.J., O'Higgins, P., 2016. Validity and sensitivity of
830 a human cranial finite element model: implications for comparative studies of biting
831 performance, *J Anat* 228, 70-84.
- 832 Toro-Ibacache, V., Zapata Muñoz, V., O'Higgins, P., 2015. The Predictability from Skull
833 Morphology of Temporalis and Masseter Muscle Cross-Sectional Areas in Humans, *The*
834 *Anatomical Record* 298, 1261-1270.
- 835 Trinkaus, E., 1987. The Neandertal Face - Evolutionary and Functional Perspectives on a
836 Recent Hominid Face, *J Hum Evol* 16, 429-443.
- 837 Wang, Q.A., Smith, A.L., Strait, D.S., Wright, B.W., Richmond, B.G., Grosse, I.R., Byron,
838 C.D., Zapata, U., 2010. The Global Impact of Sutures Assessed in a Finite Element Model of
839 a Macaque Cranium, *Anat Rec* 293, 1477-1491.
- 840 Weber, G.W., 2015. *Virtual Anthropology*, *Am J Phys Anthropol* 156, 22-42.
- 841 Weber, G.W., Bookstein, F.L., 2011. *Virtual Anthropology - A Guide for a New*
842 *Interdisciplinary Field*, Springer-Verlag, Wien.
- 843 Weijjs, W.A., 1980. Biomechanical Models and the Analysis of Form: A Study of the
844 Mammalian Masticatory Apparatus, *Am Zool* 20, 707-719.
- 845 Wilczek, J., Monna, F., Barral, P., Burlet, L., Chateau, C., Navarro, N., 2014. Morphometrics
846 of Second Iron Age ceramics – strengths, weaknesses, and comparison with traditional
847 typology, *J Archaeol Sci* 50, 39-50.
- 848 Wood, S.A., Strait, D.S., Dumont, E.R., Ross, C.F., Grosse, I.R., 2011. The effects of
849 modeling simplifications on craniofacial finite element models: The alveoli (tooth sockets)
850 and periodontal ligaments, *J Biomech* 44, 1831-1838.

- 851 Wroe, S., 2008. Cranial mechanics compared in extinct marsupial and extant African lions
852 using a finite-element approach, *J Zool* 274, 332-339.
- 853 Wroe, S., Ferrara, T.L., McHenry, C.R., Curnoe, D., Chamoli, U., 2010. The
854 craniomandibular mechanics of being human, *P Roy Soc B-Biol Sci* 277, 3579-3586.
- 855 Wroe, S., Moreno, K., Clausen, P., Mchenry, C., Curnoe, D., 2007. High-resolution three-
856 dimensional computer simulation of hominid cranial mechanics, *Anat Rec* 290, 1248-1255.
- 857 Zollikofer, C.P., Ponce de León, M.S., 2005. Virtual reconstruction: a primer in computer-
858 assisted paleontology and biomedicine, Wiley-Interscience, New Jersey.
- 859
- 860

861



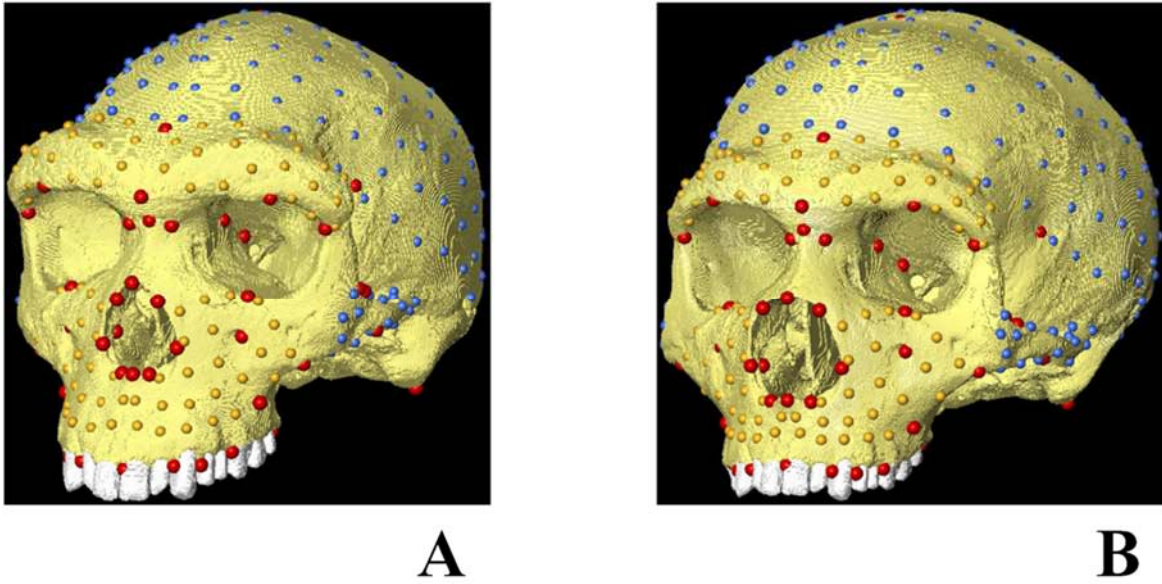
862

863 Figure 1: Cranium of Kabwe 1 (A) before and (B) after reconstruction.

864

865

866



867

868 Figure 2: A reconstructed Kabwe 1, *Homo heidelbergensis* cranium model (A) and a
869 hypothetical *Homo neanderthalensis* (B). The hypothetical Neanderthal was created via
870 surface warping model A into a mean Neanderthal landmark data set (B) using thin plate
871 splines based on classical and sliding semi-landmarks. Conventional landmarks (red spheres);
872 sliding semi-landmarks on the maxilla and brow-ridge (yellow spheres); sliding semi-
873 landmarks of the vault and zygoma (light blue spheres).

874

875
876
877
878
879
880
881
882
883
884
885
886
887
888
889
890
891
892
893
894
895
896
897
898
899

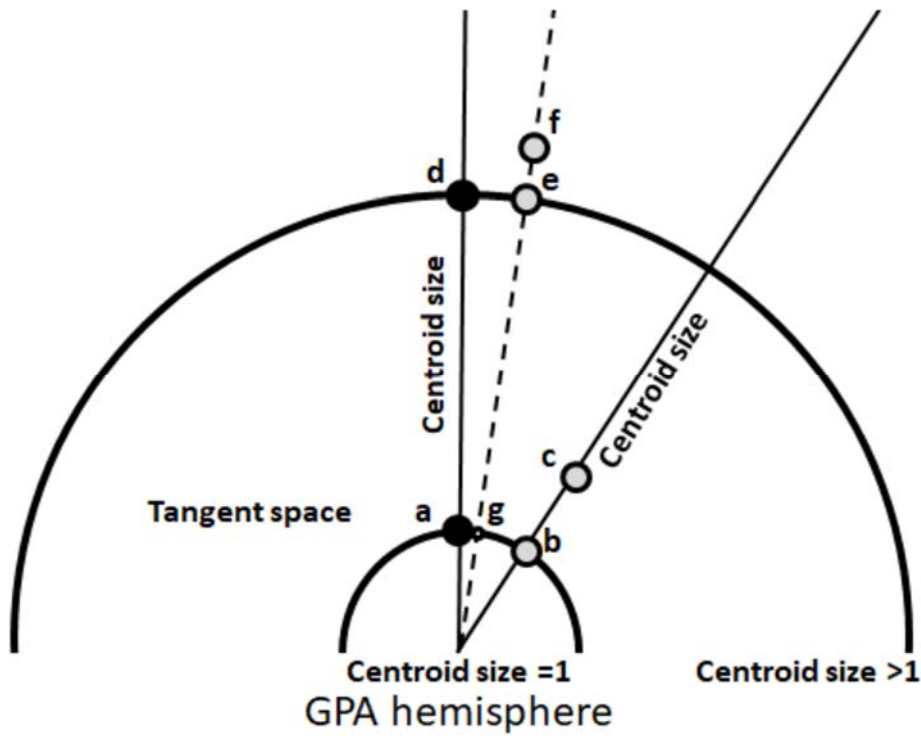


Figure 3: A schematic illustrating the hemisphere of GPA aligned coordinates (Slice 2001) for triangles, showing the tangent space, the vectors of centroid size, and the size and shape space resulting from rescaling of GPA registered coordinates to centroid size >1 . The black points, a and b, represent the same unloaded forms with different centroid sizes. The grey points c and f represent the loaded forms and the grey points b and e represent their projections onto the GPA hemispheres with centroid sizes $=1$ and >1 . G is the projection of f and e onto the GPA hemisphere with centroid size $=1$. See text for explanation.

900

901

902 Figure 4: PCA of large scale deformations of a sensitivity study assessing the impact of
903 simplifications of material properties in a modern human cranium. Model 1 is not visible
904 because it is in the same location in the plot as model 2. Deformations are magnified by a
905 factor of 500 to facilitate visualisation.

906

907